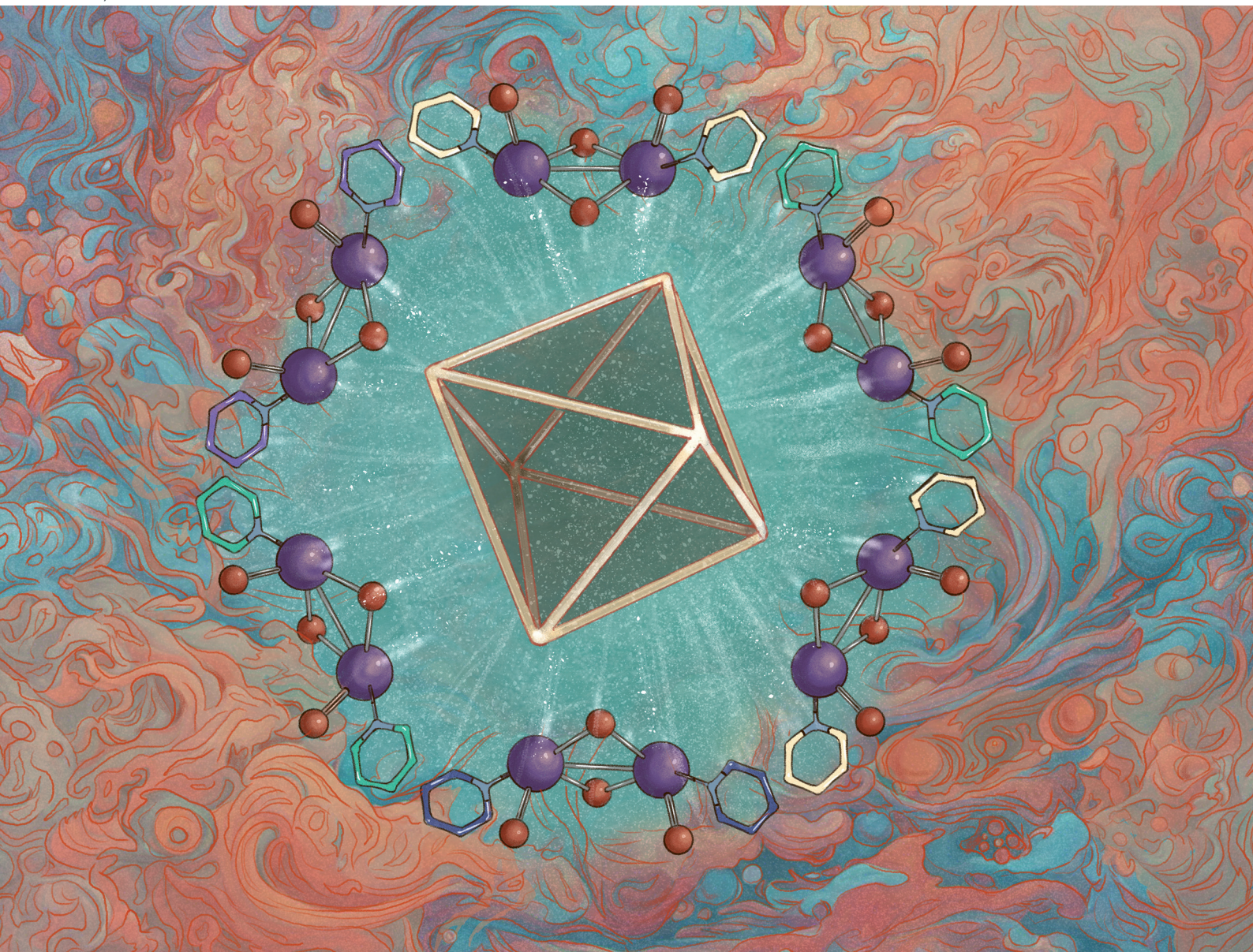


# Dalton Transactions

An international journal of inorganic chemistry

rsc.li/dalton



ISSN 1477-9226

**PAPER**







Guillermo Mínguez Espallargas *et al.*  
Imparting structural robustness of metal-organic cages  
based on oxo-dimolybdenum clusters

Cite this: *Dalton Trans.*, 2023, **52**, 15682Received 1st August 2023,  
Accepted 21st August 2023

DOI: 10.1039/d3dt02482b

rsc.li/dalton

# Imparting structural robustness of metal–organic cages based on oxo-dimolybdenum clusters†

Solène Delaporte, <sup>a,b</sup> Isabel Abánades Lázaro, <sup>a</sup> Javier López-Cabrelles, <sup>‡a</sup>  
Eleni C. Mazarakioti, <sup>a</sup> Sarah Chebourou,<sup>a</sup> Iñigo J. Vitórica-Yrezábal,<sup>c</sup>  
Mónica Giménez-Marqués <sup>a</sup> and Guillermo Mínguez Espallargas <sup>\*a</sup>

A family of robust and stable molybdenum-based metal–organic cages have been obtained based on the  $[\text{Mo}_2\text{O}_2(\mu_2\text{-O})_2]^{2+}$  secondary building unit. The resulting cages are decorated with different pyridine derivatives that impart structural stability, resulting in the structural elucidation of the activated cage with single-crystal diffraction. The chemical robustness of the cage is also demonstrated by the post-synthetic modification of the cage, which allows the exchange of the pyridine derivatives without rupture of the cage.

## Introduction

Metal–Organic Cages (MOCs) are a subclass of hybrid compounds composed of metal ions or clusters linked by organic ligands forming discrete porous molecular structures. Although MOCs have been known for over two decades,<sup>1</sup> they have attracted recent interest due to their solubility, surpassing the processability of Metal–Organic Frameworks (MOFs), their higher dimensional equivalents. In fact, MOCs have shown promising applicability for gas storage,<sup>2,3</sup> catalysis,<sup>4</sup> molecular separation<sup>5</sup> or biomedicine,<sup>6</sup> among others. Efforts have been devoted to designing crystalline MOCs with permanent porosity,<sup>7</sup> which can arise both from their inherent molecular pore space or from the packing of MOC molecules. Nevertheless, the study of MOCs remains challenging due to their poor thermal and hydrolytic stability that arises from the lack of extended connectivity.<sup>8</sup> Thus, crystals of MOCs often degrade upon activation preventing the structural determination by single crystal X-ray diffraction. This lack of structural data of activated structures hinders precise analysis and understanding of their porosity. In this context, two different scenarios

are generally found upon MOCs' activation: (i) sample amorphization;<sup>8</sup> and (ii) changes on crystallinity envisioned in PXRD patterns<sup>9</sup> but unable to provide structural information. The retention of the crystal packing upon desolvation is extremely rare.<sup>10</sup>

In most cases, the absence of structural data is substituted by Mass Spectrometry measurements, although this technique does not ensure the structural integrity of the material or the maintained packing. In some cases, this has been resolved with adsorption measurements, proving the inherent molecular pore space. Nevertheless, new approaches to obtain direct structural visualisation of the activated MOCs is needed for the development of the field.

Aiming to circumvent the lack of structural evidence of the activated samples, two alternative approaches have been developed. One of these is the assembly of MOCs *via* bidentate ligands,<sup>11–15</sup> such as dabco ligands that coordinate to the exterior of the MOCs, connecting them in a 3D manner,<sup>16</sup> analogous to dabco-pillared MOFs. Another approach is the post-synthetic assembly of MOCs into extended networks<sup>17</sup> using secondary building units (clusters) to form analogous MOFs through rigid bridges.<sup>18–20</sup> However, although these methods provide meaningful information, direct structural visualisation of the activated MOCs would be the ultimate tool to understand their porosity and gas adsorption properties.

Herein, we report the synthesis of a novel family of pyridine capped  $\text{Mo}_2$ -benzene tricarboxylate MOCs, **MUV-27** (MUV = Material of the University of Valencia), which can be obtained through a simple self-assembly synthetic route. Contrary to the previous Mo-MOCs,<sup>21–25</sup> the **MUV-27** family exhibit an original geometry that is not based on a paddlewheel unit, unstable in the case of Mo(II), but on a  $[\text{Mo}_2\text{O}_2(\mu_2\text{-O})_2]^{2+}$  core. In addition, this family of MOCs can be functionalized through the use of

<sup>a</sup>Instituto de Ciencia Molecular (ICMol), Universitat de València, Catedrático José Beltrán 2, 46980 Paterna, Spain. E-mail: guillermo.minguez@uv.es

<sup>b</sup>ENS Paris-Saclay, Département de Chimie, 4 Av. des Sciences, 91190 Gif-sur-Yvette, France

<sup>c</sup>School of Chemistry, University of Manchester, Oxford Road, Manchester M13 9PL, UK

† Electronic supplementary information (ESI) available: Containing experimental conditions and detailed characterisation. CCDC 2258028–2258034. For ESI and crystallographic data in CIF or other electronic format see DOI: <https://doi.org/10.1039/d3dt02482b>

‡ Current address: Institute for Integrated Cell–Material Sciences (WPI-iCeMS), Kyoto University Yoshida, Sakyo-ku, Kyoto 606-8501, Japan.



different auxiliary ligands (based on pyridine) which results, in one specific case, in an enhancement of the MOC structural stability, allowing the structural elucidation of the activated samples using single crystal X-ray diffraction. Thus, we unequivocally determine the retention of the cage structure upon removal of all solvents.

## Results and discussion

### Synthesis and structural study

The solvothermal reaction in dimethylformamide (DMF) of molybdenum acetate  $[\text{Mo}_2(\text{OAc})_4]$  and trimesic acid ( $\text{H}_3\text{BTC}$ ) in the presence of pyridine (py) results in a mixture of orange crystals and red gel from which single crystals could be isolated and purified. The hexagonal crystals crystallized in the monoclinic  $P2_1/c$  space group (see details in section S2 in the ESI†). Structure solution from single crystal diffraction data revealed a MOC, namely **MUV-27-py**. The secondary-building unit of this cage is formed by a dimolybdenum-oxo cluster  $[\text{Mo}_2\text{O}_2(\mu_2\text{-O})_2]^{2+}$ , denoted  $[\text{Mo}_2\text{O}_4]^{2+}$ , in which two bonded molybdenum atoms bearing oxo-ligands are connected by a non-planar double oxygen bridge (Fig. 1a). Six bimetallic  $\text{Mo}_2$ -units are located at the vertices of an irregular octahedron of approximately 10–11 Å diameter (see Fig. 1b), and form two antiparallel equilateral triangles, which are approximately 6.5 Å apart (see Fig. 1c). The six remaining isosceles triangles faces are occupied by the  $\text{BTC}^{3-}$  linkers that connect the  $\text{Mo}_2$ -units together, with the overall structure displaying a triangular antiprismatic geometry.

The bimetallic  $[\text{Mo}_2\text{O}_4]^{2+}$  fragment is a structural unit that has been commonly observed in Mo(v) chemistry. Indeed, numerous complexes containing  $[\text{Mo}_2\text{O}_4]^{2+}$  centres have been investigated,<sup>26</sup> with bond-distances that are comparable with those obtained from SXRD data of **MUV-27-py**.<sup>27</sup> The Mo–Mo distances (Table S3†) are in the range of 2.547(1)–2.555(1) Å, suggesting a single-bond between the two Mo(v) atoms. The Mo=O linkages exhibit distances in the range of 1.679(8)–

1.690(8) Å and the oxo-bridges have the Mo–O distance between 1.917(6) and 1.941(7) Å, which are also in the typical range for other reported  $[\text{Mo}_2\text{O}_4]^{2+}$  clusters.<sup>27</sup> To complete the distorted octahedral environment of the Mo centres, one pyridine is coordinated to each metal, with Mo–N bond lengths in the range 2.230(1)–2.248(9) Å. Three  $\text{BTC}^{3-}$  are coordinated to the  $[\text{Mo}_2\text{O}_4]^{2+}$  unit, two of them having an equatorial monodentate coordination mode to each metal, and the third linker is bridging both Mo atoms, in an axial *syn,syn* bidentate manner.

Therefore, **MUV-27-py** contains one  $\text{BTC}^{3-}$  linker per  $[\text{Mo}_2\text{O}_4]^{2+}$  unit and, as indicated by the structural measurements, the presence of dimethylammonium ( $\text{DMA}^+$ ) cation balances the charge. This counteranion is located in the periphery of the cavity, with the  $\text{NH}_2^+$  group forming N–H...O hydrogen bonds with the two non-coordinated oxygen atoms of the  $\text{BTC}^{3-}$  linker (Fig. 1a). <sup>1</sup>H NMR studies confirm the presence of 6  $\text{DMA}^+$  per cage, suggesting that **MUV-27-py** is a –6 negatively charged MOC of general formula  $(\text{DMA})_6[\text{Mo}_{12}\text{O}_{12}(\mu_2\text{-O})_{12}(\text{BTC})_6(\text{py})_{12}]^{6-}$ , which is further confirmed with additional characterization including PXRD, FT-IR, acid-digested <sup>1</sup>H NMR, TGA and UV-vis studies (see sections S3–S8 in the ESI†).

### Functionalization of MUV-27

As commonly found in MOCs, activation of **MUV-27-py** causes a change in the crystal packing, as evidenced by X-ray powder diffraction (Fig. S16†). In fact, structural changes are also observed simply upon drying the materials (Fig. S8†). In order to circumvent these issues, the supramolecular packing structure was reinforced by introducing functionalised capping ligands during the synthesis. Thus, following the same synthetic procedure as for **MUV-27-py**, three functionalized MOCs have been synthesized using 4-picoline ( $\text{py-CH}_3$ ), 1,2-bis(4-pyridyl)ethane ( $\text{bpy-C}_2$ ) and 1,3-bis(4-pyridyl)propane ( $\text{bpy-C}_3$ ), resulting in three new MOCs denoted **MUV-27-py-CH<sub>3</sub>**, **MUV-27-bpy-C<sub>2</sub>** and **MUV-27-bpy-C<sub>3</sub>**, respectively. These MOCs were also obtained as single-crystals, thus allowing their struc-

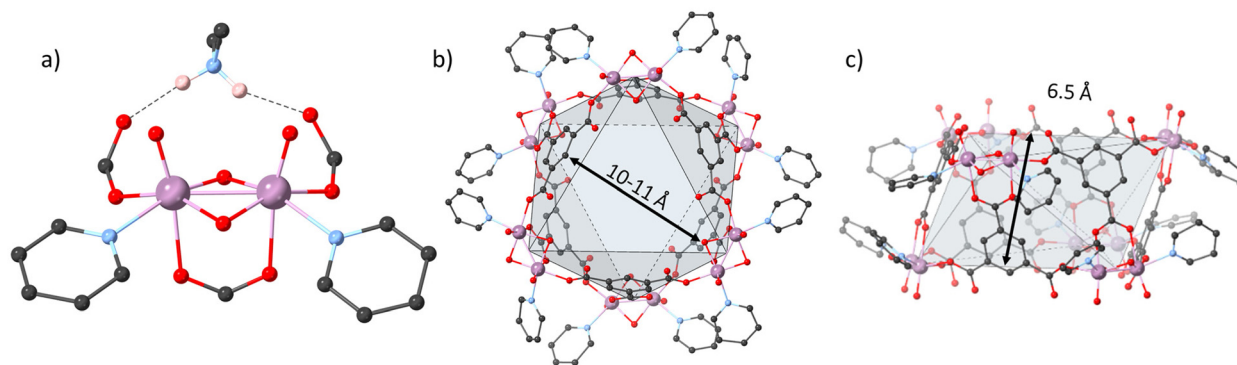


**Fig. 1** (a) Single-building unit of **MUV-27-py** containing the  $[\text{Mo}_2\text{O}_4]^{2+}$  cluster and one  $\text{DMA}^+$  cation; (b) and (c) orthogonal views of the structure of the octahedral  $[\text{Mo}_{12}\text{O}_{12}(\mu_2\text{-O})_{12}(\text{BTC})_6(\text{py})_{12}]^{6-}$  cage, **MUV-27-py**. Colour code: Mo = pink, O = red, C = black, N = blue. Hydrogen atoms have been omitted for clarity except those of the  $\text{DMA}^+$  cation in a.



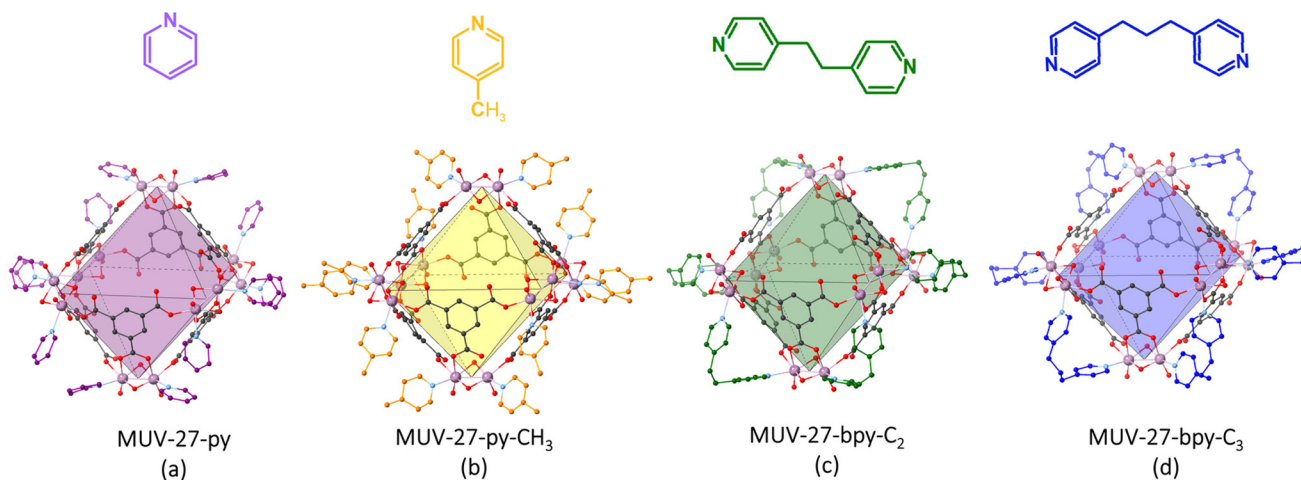


Fig. 2 Structures of MUV-27 with different capping ligands (shown in different colours): (a) MUV-27-py; (b) MUV-27-py-CH<sub>3</sub>; (c) MUV-27-bpy-C<sub>2</sub>; (d) MUV-27-bpy-C<sub>3</sub>.

tural elucidation revealing, in the three cases, “Mo<sub>12</sub>” MOCs analogous to MUV-27-py (Fig. 2), with molecular formulas (DMA)<sub>6</sub>[Mo<sub>12</sub><sup>V</sup>O<sub>12</sub>(μ<sub>2</sub>-O)<sub>12</sub>(BTC)<sub>6</sub>(py-CH<sub>3</sub>)<sub>12</sub>], (DMA)<sub>6</sub>[Mo<sub>12</sub><sup>V</sup>O<sub>12</sub>(μ<sub>2</sub>-O)<sub>12</sub>(BTC)<sub>6</sub>(bpy-C<sub>2</sub>)<sub>6</sub>] and (DMA)<sub>6</sub>[Mo<sub>12</sub><sup>V</sup>O<sub>12</sub>(μ<sub>2</sub>-O)<sub>12</sub>(BTC)<sub>6</sub>(bpy-C<sub>3</sub>)<sub>6</sub>]. Remarkably, the cages with bipyridine ligands (bpy-C<sub>2</sub> and bpy-C<sub>3</sub>) were not assembled together forming MOFs or amorphous supramolecular soft polymers as previously reported with other MOCs and similar bidentate ligands,<sup>12,15,20</sup> but instead each ditopic ligand bridged two molybdenum atoms from neighbouring [Mo<sub>2</sub>O<sub>4</sub>]<sup>2+</sup> fragments of the same cage (Fig. 2c and d). Importantly, activation of these three MOCs is accompanied by retention of crystallinity (Fig. S16<sup>†</sup>), but the crystal packing is not maintained likely caused from a re-organization of the MOCs, which unfortunately could not be followed by single crystal diffraction.

In order to overcome the structural arrangement observed in the previous MUV-27 materials upon activation, a ligand with potentially increased supramolecular interactions was used, namely 4-aminopyridine (py-NH<sub>2</sub>). Following a similar synthetic protocol results in homogeneous red rhombohedral crystals of MUV-27-py-NH<sub>2</sub>-DMF, which also forms Mo<sub>12</sub> MOCs analogous to the previous compounds. However, in this case a DMF molecule is coordinated to a Mo atom substituting a py-NH<sub>2</sub> ligand (Fig. S6<sup>†</sup>), leading to the molecular formula (DMA)<sub>6</sub>[Mo<sub>12</sub><sup>V</sup>O<sub>12</sub>(μ<sub>2</sub>-O)<sub>12</sub>(BTC)<sub>6</sub>(py-NH<sub>2</sub>)<sub>11</sub>(DMF)]. Close inspection of the crystal packing reveals the presence of N-H...O hydrogen bonds (2.073–2.694 Å range) between the amino-groups and oxygen atoms from surrounding cages (Fig. 3). Activation of MUV-27-py-NH<sub>2</sub>-DMF crystals was successfully achieved in a two-step process: (1) DMF solvent molecules were replaced by DCM *via* washing, direct soaking for 2 days and further washing, leading to single crystals that were analysed by X-ray single crystal diffraction. We could observe a significant decrease in the *a* and *b* unit cell parameters, although minor changes in the crystal packing had occurred (see Table 1 and Fig. 4). (2) Then, these crystals containing DCM

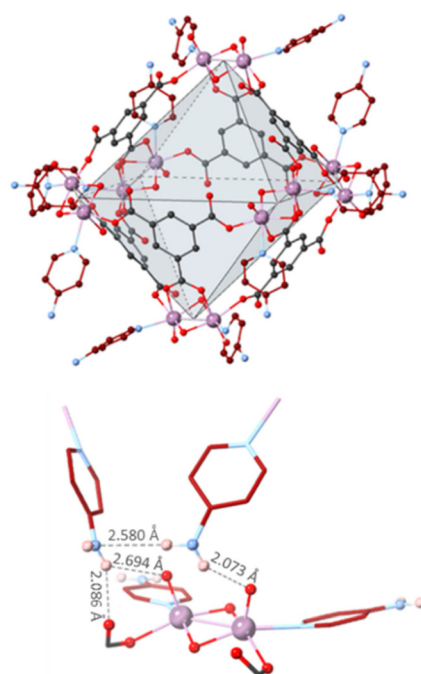


Fig. 3 (top) Structure of MUV-27-py-NH<sub>2</sub>; (bottom) H-bonds between the [Mo<sub>2</sub>O<sub>4</sub>]<sup>2+</sup> subunit of one MOC and 4-aminopyridine ligands of a different MOC.

Table 1 Parameters extracted from X-ray single crystal diffraction of MUV-27-py-NH<sub>2</sub>

Parameter	DMF	DCM	act
<i>a</i> /Å	19.7115(3)	19.3279(4)	19.0877(7)
<i>b</i> /Å	20.0909(2)	19.6862(3)	18.2843(6)
<i>c</i> /Å	27.2180(4)	27.2810(10)	26.7480(7)
<i>β</i> /°	110.345(2)	109.113(3)	108.715(3)
Space group	<i>P</i> 2 <sub>1</sub> / <i>n</i>	<i>P</i> 2 <sub>1</sub> / <i>n</i>	<i>P</i> 2 <sub>1</sub> / <i>n</i>



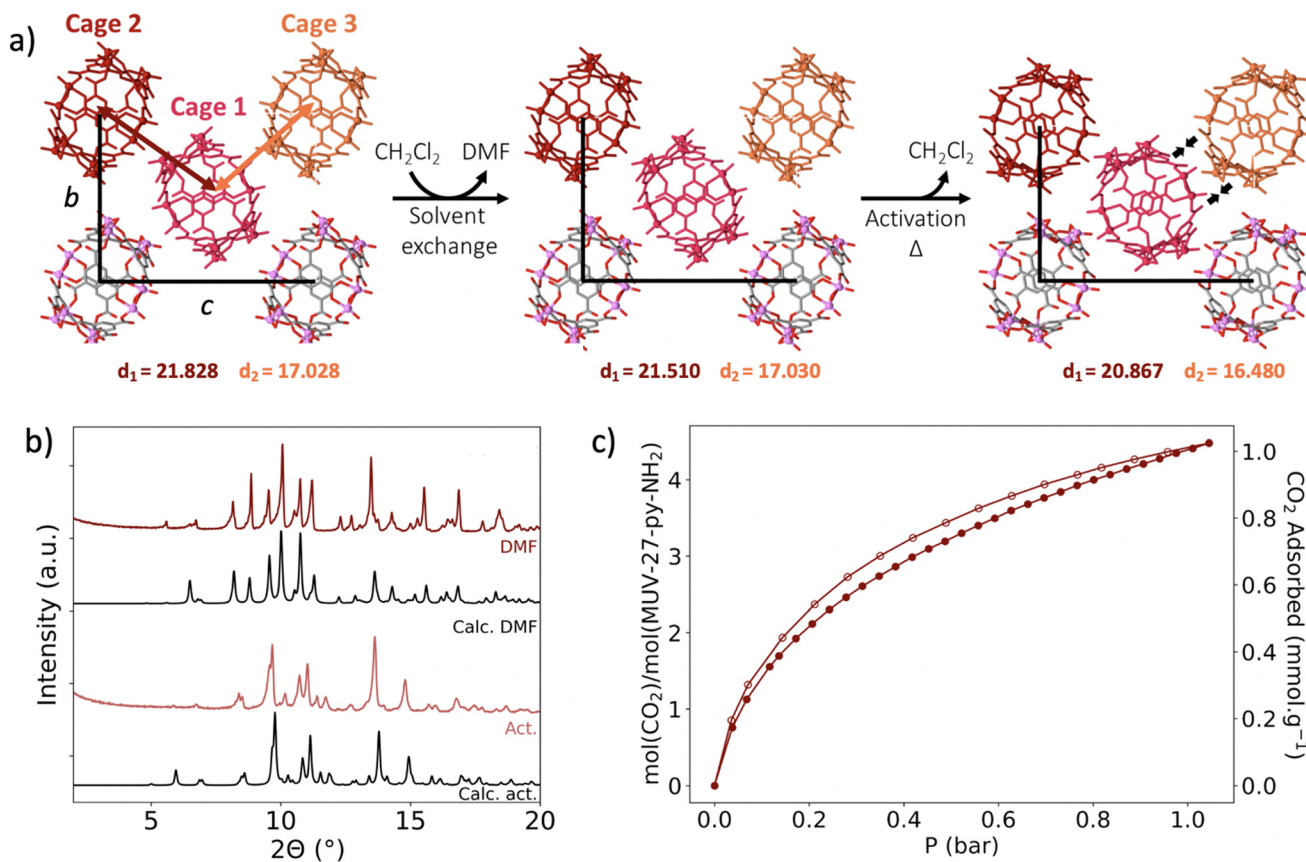


Fig. 4 (a) Evolution of MUV-27-py-NH<sub>2</sub> unit cell along the a-axis upon solvent exchange and activation; (b) calculated and experimental PXRD patterns of MUV-27-py-NH<sub>2</sub> in DMF and after desolvation; (c) CO<sub>2</sub> adsorption (filled circles) desorption (empty circles) isotherms at 273 K of activated MUV-27-py-NH<sub>2</sub>.

molecules were dried at air for 24 hours, obtaining the activated compound, denoted **MUV-27-py-NH<sub>2</sub>-act**. Despite of the two-step transformation, suitable single crystals for X-ray diffraction of the activated product were isolated, allowing to obtain unequivocal evidence of the structural changes suffered in the activation process of **MUV-27-py-NH<sub>2</sub>-DMF**. Thus, while the cage's molecular structure is maintained with minor deformations, the crystal packing is affected significantly (see section S2.7 in the ESI†), with a shortening in the intermolecular distances as shown in Fig. 4a, which is translated in a reduction of the unit cell parameters (*a*, *b* and *c*). Nevertheless, the typical crystal collapse that is normally observed upon activation has been avoided, likely due to the presence of N-H...O hydrogen bonds between MOCs, that have reinforced the overall crystal stability.

Subsequently, the porosity of the activated **MUV-27-py-NH<sub>2</sub>-act** (activation procedure as for the SCXRD measurements) was investigated through N<sub>2</sub> and CO<sub>2</sub> isotherms, at 77 K and 273 K respectively. While N<sub>2</sub> adsorption was almost negligible (Fig. S28†), moderate CO<sub>2</sub> sorption was observed (Fig. 4c), with *ca.* 4 molecules of CO<sub>2</sub> per cage, demonstrating the retention of porosity upon activation. Interestingly, the other MOCs also show some CO<sub>2</sub> sorption capacity (Fig. S29†), indicating that the intrinsic porosity of the cages is accessible upon activation.

Finally, an important aspect for the use of MOCs is their robustness upon application of chemical stimuli. In this sense, despite the ample number of cages that has been reported, there is only one example of a Rh-based cage has been shown to be robust enough to make composites.<sup>28</sup> Thus, we examined the robustness of these Mo-based cages in order to enhance the chemical variety of stable MOCs. For this, we evaluated the robustness and effects of post-synthetic modification (PSM)<sup>28–33</sup> in the **MUV-27** family of cages, by preparing a suspension of the insoluble cages in DMF with the solubilized pyridine capping ligands and heating at 50 °C upon stirring overnight. In particular, the transformation of **MUV-27-py** and **MUV-27-py-CH<sub>3</sub>** to all the aforementioned materials was successful, leading to crystalline materials with a complete exchange of the pyridine capping ligands confirmed by <sup>1</sup>H NMR, PXRD and FT-IR (section S11 in the ESI†). However, when using other **MUV-27** cages as synthetic platforms (*i.e.* **MUV-27-bpy-C<sub>2</sub>**, **MUV-27-bpy-C<sub>3</sub>** and **MUV-27-NH<sub>2</sub>**), only a partial exchange of the ligands was observed, possibly due to the bis-coordination mode of the capping ligands in **MUV-27-bpy-C<sub>2</sub>**, **MUV-27-bpy-C<sub>3</sub>** and to the H-bonding of the NH<sub>2</sub> group in **MUV-27-py-NH<sub>2</sub>**. This successful PSMs prove the chemical robustness of the cages and could also be used as a platform multi-functionalised MOCs.



## Conclusions

A novel family of metal–organic cages composed of 12 Mo(v) centres, denoted **MUV-27**, has been prepared bearing a novel secondary building unit in MOC chemistry,  $[\text{Mo}_2\text{O}_2(\mu_2\text{-O})_2]^{2+}$ . The general synthetic approach is demonstrated with the preparation of five different compounds possessing different functional groups. Pure and crystalline cages can be easily obtained through a self-assembly synthesis and functionalized with pyridine derivatives. Importantly, the introduction of  $-\text{NH}_2$  groups enhances the structural stability of the resultant MOC through hydrogen bonding between cages, resulting in crystals suitable for structural determination after activation. This important aspect has been elusive despite the large interest in this type of compounds. Specifically, we unequivocally demonstrate that the  $\text{Mo}_{12}$  **MUV-27-py-NH<sub>2</sub>** MOC is structurally robust upon activation, despite the effective shrinkage of the crystal packing. We have also confirmed the possibility to conduct post-synthetic modifications on **MUV-27** cages, which is encouraging in the prospect of future experiments to tune the functionalities of **MUV-27** and highlights the robustness of the cages.

These results evidence the plausible retainment of structural integrity in MOCs which enables direct determination of the crystal structure. Therefore, we believe that the methods here reported –enhancing stability through inter-cages interactions between functionalised ligands– could have applicability in other MOC systems.

## Conflicts of interest

There are no conflicts to declare.

## Acknowledgements

The work has been supported by the European Union (ERC-2016-CoG 724681-S-CAGE), grants PID2020-117177GB-I00, PID2020-118564GA-I00 and CEX2019-000919-M, funded by MCIN/AEI/10.13039/501100011033, and the Generalitat Valenciana (CIPROM/2022/48). This study forms part of the Advanced Materials program and was supported by MCIN with funding from European Union NextGenerationEU (PRTR-C17.I1) and by Generalitat Valenciana (project MAF/2022/31). M. G.-M, and I. A.-L. thank MICINN for a Ramón y Cajal fellowship (RYC2019-027902-I), a Juan de la Cierva Incorporación fellowship (IJC2020-044374-I), respectively. J. L.-C. acknowledges the Universitat de València for an “Atracció de Talent” grant.

## References

- D. Zhang, T. K. Ronson, Y.-Q. Zou and J. R. Nitschke, *Nat. Rev. Chem.*, 2021, **5**, 168–182.
- A. C. Sudik, A. R. Millward, N. W. Ockwig, A. P. Côté, J. Kim and O. M. Yaghi, *J. Am. Chem. Soc.*, 2005, **127**, 7110–7118.
- S. Furukawa, N. Horike, M. Kondo, Y. Hijikata, A. Carné-Sánchez, P. Larpent, N. Louvain, S. Diring, H. Sato, R. Matsuda, R. Kawano and S. Kitagawa, *Inorg. Chem.*, 2016, **55**, 10843–10846.
- L. Chen, T. Yang, H. Cui, T. Cai, L. Zhang and C.-Y. Su, *J. Mater. Chem. A*, 2015, **3**, 20201–20209.
- D. Zhang, T. K. Ronson, Y.-Q. Zou and J. R. Nitschke, *Nat. Rev. Chem.*, 2021, **5**, 168–182.
- H. Sepehrpour, W. Fu, Y. Sun and P. J. Stang, *J. Am. Chem. Soc.*, 2019, **141**, 14005–14020.
- A. J. Gosselin, C. A. Rowland and E. D. Bloch, *Chem. Rev.*, 2020, **120**, 8987–9014.
- S. Mollick, S. Fajal, S. Mukherjee and S. K. Ghosh, *Chem. – Asian J.*, 2019, **14**, 3096–3108.
- B. Lerma-Berlanga, J. Castells-Gil, C. R. Ganivet, N. Almora-Barrios, J. González-Platas, O. Fabelo, N. M. Padial and C. Martí-Gastaldo, *J. Am. Chem. Soc.*, 2021, **143**, 21195–21199.
- (a) M. Zhou, G. Liu, Z. Ju, K. Su, S. Du, Y. Tan and D. Yuan, *Cryst. Growth Des.*, 2020, **20**, 4127–4134; (b) C. A. Rowland, G. R. Lorz, A. J. Gosselin, B. A. Trump, G. P. A. Yap, C. M. Brown and E. D. Bloch, *J. Am. Chem. Soc.*, 2018, **140**, 11153–11157.
- H.-J. Jung, D.-H. Moon and H.-P. Chun, *Bull. Korean Chem. Soc.*, 2011, **32**, 2489–2492.
- A. Carné-Sánchez, G. A. Craig, P. Larpent, T. Hirose, M. Higuchi, S. Kitagawa, K. Matsuda, K. Urayama and S. Furukawa, *Nat. Commun.*, 2018, **9**, 2506.
- A. Legrand, L.-H. Liu, P. Royla, T. Aoyama, G. A. Craig, A. Carné-Sánchez, K. Urayama, J. J. Weigand, C.-H. Lin and S. Furukawa, *J. Am. Chem. Soc.*, 2021, **143**, 3562–3570.
- A. Carné-Sánchez, G. A. Craig, P. Larpent, V. Guillerm, K. Urayama, D. Maspocho and S. Furukawa, *Angew. Chem., Int. Ed.*, 2019, **58**, 6347–6350.
- Z. Wang, C. V. Santos, A. Legrand, F. Haase, Y. Hara, K. Kanamori, T. Aoyama, K. Urayama, C. M. Doherty, G. J. Smiles, B. R. Pauw, Y. J. Colón and S. Furukawa, *Chem. Sci.*, 2021, **12**, 12556–12563.
- G. R. Lorz, A. J. Gosselin, B. A. Trump, A. H. P. York, A. Sturluson, C. A. Rowland, G. P. A. Yap, C. M. Brown, C. M. Simon and E. D. Bloch, *J. Am. Chem. Soc.*, 2019, **141**, 12128–12138.
- A. Khobotov-Bakishev, L. Hernández-López, C. von Baeckmann, J. Albalad, A. Carné-Sánchez and D. Maspocho, *Adv. Sci.*, 2022, **9**, 2104753.
- A. Khobotov-Bakishev, C. von Baeckmann, B. Ortín-Rubio, L. Hernández-López, A. Cortés-Martínez, J. Martínez-Esaín, F. Gándara, J. Juanhuix, A. E. Platero-Prats, J. Faraudo, A. Carné-Sánchez and D. Maspocho, *J. Am. Chem. Soc.*, 2022, **144**, 15745–15753.
- T. Grancha, A. Carné-Sánchez, F. Zarekarizi, L. Hernández-López, J. Albalad, A. Khobotov, V. Guillerm, A. Morsali, J. Juanhuix, F. Gándara, I. Imaz and D. Maspocho, *Angew. Chem., Int. Ed.*, 2021, **60**, 5729–5733.
- J.-R. Li, D. J. Timmons and H.-C. Zhou, *J. Am. Chem. Soc.*, 2009, **131**, 6368–6369.



- 21 Y. Ke, D. J. Collins and H.-C. Zhou, *Inorg. Chem.*, 2005, **44**, 4154–4156.
- 22 J.-R. Li, A. A. Yakovenko, W. Lu, D. J. Timmons, W. Zhuang, D. Yuan and H.-C. Zhou, *J. Am. Chem. Soc.*, 2010, **132**, 17599–17610.
- 23 F. A. Cotton, L. M. Daniels, C. Lin, C. A. Murillo and C. A. Murillo, *Chem. Commun.*, 1999, 841–842.
- 24 G. R. Lorz, A. J. Gosselin, B. S. Lindner, R. Bhattacharjee, G. P. A. Yap, S. Caratzoulas and E. D. Bloch, *Chem. Commun.*, 2019, **55**, 9527–9530.
- 25 M. M. Deegan and E. D. Bloch, *Dalton Trans.*, 2021, **50**, 3127–3131.
- 26 H. K. Chae, W. G. Klemperer and T. A. Marquart, *Coord. Chem. Rev.*, 1993, **128**, 209–224.
- 27 B. Modéc and J. Zubieta, *Materials*, 2010, **3**, 150–157.
- 28 A. Carné-Sánchez, J. Albalad, T. Grancha, I. Imaz, J. Juanhuix, P. Larpent, S. Furukawa and D. Maspocho, *J. Am. Chem. Soc.*, 2019, **141**(9), 4094–4102.
- 29 J. Liu, Z. Wang, P. Cheng, M. J. Zaworotko, Y. Chen and Z. Zhang, *Nat. Rev. Chem.*, 2022, **6**, 339–356.
- 30 E. Sánchez-González, M. Y. Tsang, J. Troyano, G. A. Craig and S. Furukawa, *Chem. Soc. Rev.*, 2022, **51**, 4876–4889.
- 31 M. L. Schneider, O. M. Linder-Patton and W. M. Bloch, *Chem. Commun.*, 2020, **56**, 12969–12972.
- 32 M. T. Yong, O. M. Linder-Patton and W. M. Bloch, *Inorg. Chem.*, 2022, **61**, 12863–12869.
- 33 V. Brega, M. Zeller, Y. He, H. Peter Lu and J. K. Klosterman, *Chem. Commun.*, 2015, **51**, 5077–5080.

